Modern Physics Letters B, Vol. 5, No. 26 (1991) 1713–1725

WEAK MEASUREMENTS

J. G. STORY, N. W. M. RITCHIE, and R. G. HULET
Department of Physics and Rice Quantum Institute,
Rice University, Houston, Texas 77251-1892, USA

Received 1 November 1991

A general description of weak measurements is presented. The "weak value" of an operator in pre- and post-selected systems is described both mathematically and using physical arguments. An optical experiment in which a measurement of a weak value has been realized is described. The possible use of pre- and post-selection as a means to amplify and detect weak effects is also discussed.

1. Introduction

A measurement in quantum mechanics generally consists of two elements, a measuring device and the system to be measured. In an ideal measurement, the interaction between these two elements results in the measurement of an eigenvalue of an observable of the system and the system is left in an eigenstate of the measured observable. Any subsequent measurement of the same observable on the same system will produce the same result. In a non-ideal measurement incomplete information is obtained. The measurement does not leave the system in one eigenstate of the observable. Recent theoretical and experimental work has examined this class of measurements which have been called "weak measurements".[1]

Weak measurements are of fundamental interest because quantum mechanical measurements are never ideal. The strength of a measurement can be rated on a scale from zero to one, where zero gives no information about the observable and one is an ideal measurement in which the observable is determined exactly. As all experimental measurements fall somewhere between zero and one on this scale, an understanding of non-ideal measurements is important in understanding the quantum mechanical measurement process.

In a recent series of articles discussing weak measurements,[1–5] the concept of a "weak value" was introduced. The weak value involves a weak measurement performed on systems during the time between a pre- and post-selection. The pre- and post-selections are accomplished via nearly ideal measurements which select a particular eigenstate of an observable. The concept of weak values was introduced

PACS Nos.: 03.65.Bz, 42.10.Jd, and 42.10.Qj.

by Aharanov, Albert and Vaidman (AAV)[1] and demonstrated recently[6] in an optical experiment proposed by Duck, Stevenson and Sudarshan (DSS).[2] The experiment showed that under certain circumstances the weak value of an observable can be far outside the range of eigenvalues of the operator corresponding to that observable.

2. Theory

In general, a measuring device may be represented by a Hamiltonian H, which couples the measuring device with the system to be measured. This may be represented by[7]

$$H = -g(t)\hat{q}\hat{A} \tag{1}$$

where $\hat{A}$ is the operator of the observable to be measured, with eigenvalues a_i, q is the canonical variable of the measuring device with conjugate momentum p, and $g(t)$ is a function with compact support near the time of measurement which is normalized so that its integral over time is unity. In an ideal measurement of a system, the initial and final values of p are known precisely. The difference $p_f - p_i$ is equal to an eigenvalue a_i of the observable. Since q and p are conjugate variables, the uncertainty principle prevents precise knowledge of both quantities. In most measurements the uncertainty in q is large enough to achieve a sufficiently small variance in p. Since one generally has at least some knowledge of q (it will typically be bounded by experimental limitations), there is necessarily some uncertainty in p. In a weak measurement, the uncertainty in p is sufficiently large that the system is left in a superposition of eigenstates of the operator $\hat{A}$ after the measurement.[8] No unique eigenvalue a_i is measured.

To measure the weak value, systems are pre-selected via a nearly ideal measurement in some eigenstate $|\Psi_{in}\rangle$ of an observable. The systems then interact with a measuring device which is weakly coupled to the observable A. Finally, the systems are post-selected via another nearly ideal measurement in some eigenstate $|\Psi_f\rangle$ of an observable. The pre- and post-selection observables are usually chosen to be non-commuting. The weak value of an observable with operator $\hat{A}$ is defined by AAV to equal

$$A_w \equiv \frac{\langle \Psi_f | \hat{A} | \Psi_{in} \rangle}{\langle \Psi_f | \Psi_{in} \rangle} \tag{2}$$

where $\hat{A}$ is the operator of the weak measuring device. Under certain circumstances unusual results can be obtained for the weak value. In particular, if the initial and final states are nearly orthogonal, A_w can be much larger than any of the eigenvalues a_i of $\hat{A}$. This amplification of the eigenvalue separation is of both theoretical and experimental interest.

A more complete understanding of the nature of the weak value requires a formal description of the measuring process. The formalism presented here follows that of DSS.[2] For simplicity, the initial state of the measuring device in the basis of both conjugate variables, q and p, is assumed to be a Gaussian distribution.

Restriction to a Gaussian distribution is not necessary but makes the mathematics more transparent. Initially the measuring device is in a state given by

$$|\Phi_{\text{in}}\rangle = \int dq \, \exp[-q^2/4\Delta^2]|q\rangle \tag{3}$$

in the q representation and

$$|\Phi_{\text{in}}\rangle = \int dp \, \exp[-\Delta^2 p^2]|p\rangle \tag{4}$$

in the p representation. Δ is a measure of the initial uncertainty in the distribution

$$\Delta q = \Delta, \quad \Delta p = 1/(2\Delta) \tag{5}$$

with $\hbar = 1$. The systems to be measured are pre-selected in a state $|\Psi_{\text{in}}\rangle$ and post-selected in a state $|\Psi_{\text{f}}\rangle$ which can be expanded in terms of the eigenstates of $\widehat{A}$:

$$|\Psi_{\text{in}}\rangle = \sum\nolimits_i \alpha_i |A = a_i\rangle \tag{6}$$

and

$$|\Psi_{\text{f}}\rangle = \sum\nolimits_i \beta_i |A = a_i\rangle \, . \tag{7}$$

The result of the interaction of the measuring device with the system is given by

$$\begin{aligned} |\Phi_{\text{f}}\rangle &= \langle\Psi_{\text{f}}| \exp[-i \int \widehat{H} \, dt]|\Psi_{\text{in}}\rangle|\Phi_{\text{in}}\rangle \\ &= \sum\nolimits_i \alpha_i \beta_i^* \int dq \, \exp[-\Delta^2 (p - a_i)^2]|p\rangle \end{aligned} \tag{8}$$

in the p representation. For large Δ, representing a small uncertainty in p, the state of the measuring device after the interaction is a series of narrow peaks centered on the eigenvalues a_i of $\widehat{A}$. This situation constitutes a strong measurement of the system. In contrast, if Δ is small, so the uncertainty in the initial value of p is large compared to the eigenvalue spacing, the final state of the measuring device is a series of overlapping Gaussians. In this situation the eigenvalues of the operator $\widehat{A}$ are not resolved by the measurement.

It is important to note that the sum in Eq. 8 involves complex coefficients and not just a sum of squares of real numbers. Therefore, interference can occur which can dramatically effect the measured distribution. Under certain restrictions, the centroid of the distribution given by Eq. 8 is approximately located at A_{w}. This can be demonstrated as follows:

$$\begin{aligned} |\Phi_{\text{f}}\rangle &= \langle\Psi_{\text{f}}|e^{i\hat{q}\widehat{A}}|\Psi_{\text{in}}\rangle|\Phi_{\text{in}}\rangle \\ &\simeq (\langle\Psi_{\text{f}}|\Psi_{\text{in}}\rangle + i\hat{q}\,\langle\Psi_{\text{f}}|\widehat{A}|\Psi_{\text{in}}\rangle + \cdots)|\Phi_{\text{in}}\rangle \\ &= \langle\Psi_{\text{f}}|\Psi_{\text{in}}\rangle(1 + i\hat{q}A_{\text{w}} + \cdots)|\Phi_{\text{in}}\rangle \\ &\simeq \langle\Psi_{\text{f}}|\Psi_{\text{in}}\rangle \int dq \, e^{iqA_{\text{w}}} \exp[-q^2/4\Delta^2]|q\rangle \end{aligned} \tag{9}$$

where qA_w is assumed small compared to unity. Transforming to the p representation gives

$$|\Phi_f\rangle = \langle\Psi_f|\Psi_{in}\rangle \int dp \exp[-\Delta^2(p - A_w^2)]|p\rangle . \tag{10}$$

When the above approximations are valid, the sum of the shifted momentum distributions can be replaced by a single distribution shifted by A_w. Under certain pre- and post-selection conditions, A_w can be much larger than any of the eigenvalues of $\hat{A}$, due to the interference of the complex coefficients in Eq. 8.

A_w is approximately equal to the location of the centroid of the distribution only when the higher order terms in the exponential of Eq. 9 are negligible. This restriction requires

$$\Delta \gg 1/A_w \tag{11}$$

and

$$\Delta \ll |\langle\Psi_f|\hat{A}|\Psi_{in}\rangle/\langle\Psi_f|\hat{A}^n|\Psi_{in}\rangle|^{1/(n-1)} \tag{12}$$

for all $n > 1$. Consequently, A_w has physical meaning only when its value lies within the initial spread of values of p for the measuring device. A_w cannot be outside the spectrum of uncertainty of the measuring device. However, it is possible to record a signal which is well defined and centered around a value which is far outside the range of possible eigenvalues of $\hat{A}$.

The price for obtaining this rather strange result is a loss in signal size. The interference which produces the shift observed in the measurement of the weak value also reduces the signal. To obtain a large weak value, the pre- and post-selected states must be very nearly orthogonal. The weakness requirement means that the interaction, represented by the coupling Hamiltonian, only weakly perturbs the systems between the pre- and post-selection. Therefore, it becomes increasingly unlikely for systems to pass both the pre- and post-selection as the overlap between these states diminishes.

3. Interpretation

The following interpretation of the weak value has been suggested.[3,9–11] It is assumed that the pre- and post-selections are ideal measurements. Detected systems are known to have been in the state $|\Psi_{in}\rangle$ immediately after the pre-selection and in the state $|\Psi_f\rangle$ immediately after the post-selection. The wave function is well defined at those two points of time. Since the weak measurement is assumed to have a nearly negligible effect on the systems between the two selections, the systems are assumed to have the eigenvalues of their respective selected states throughout the intermediate time. We can define an operator

$$\hat{C} \equiv \hat{A} + \hat{B} \tag{13}$$

equal to the sum of the operators corresponding to the pre- and post-selection. In a normal measurement, the expectation value of $\hat{C}$ may differ greatly depending on

the time ordering of the measurements of A and B if their corresponding operators are non-commuting. However, if the interaction is sufficiently weak so that the system is negligibly effected by the measuring process, then the measurement is independent of the time ordering. In the intermediate time between the pre- and post-selection, the expectation value of $\widehat{C}$ is the sum of the expectation values A and B.

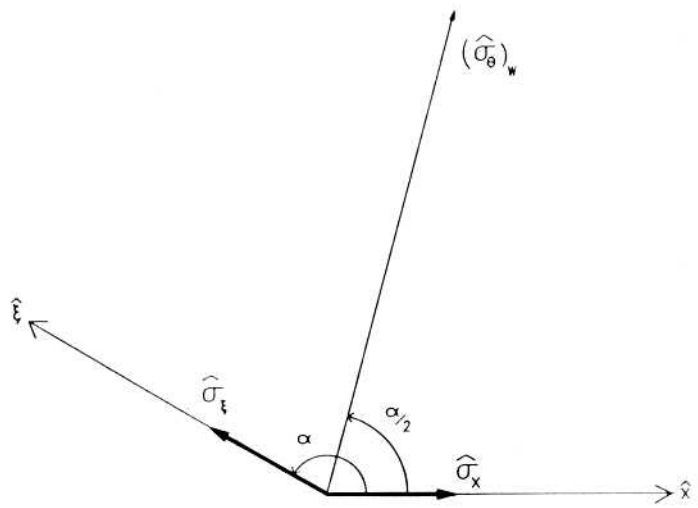

Fig. 1. The pre-selection of the spin is chosen so that all particles are initially in the spin-up state in the $\hat{x}$ direction. The post-selection selects only those particles which are finally in the spin-up state in the $\hat{\xi}$ direction, which is at an angle α with the $\hat{x}$ axis. Between the pre- and post-selections, a weak measurement of the spin component in the $\hat{\theta}$ direction is performed, where $\theta = \alpha/2$. The result of the measurement is the value $(\sigma_\theta)_w$ which is approximately equal to $[\cos(\alpha/2)]^{-1}$. As α approaches π, $(\sigma_\theta)_w$ becomes much larger than the original spin of the particles. In this figure, $\alpha = 150°$ giving $(\sigma_\theta)_w = 3.9$.

A system of spin-$\frac{1}{2}$ particles has been used to illustrate this interpretation.[3] The weak measurement is performed with a Stern-Gerlach device which gives the particles a spin dependent momentum kick. The weakness requirement is met by making the momentum kick insufficient to resolve the spin states given the transverse momentum spread of the beams. The particles travel along the $\hat{z}$ direction with the $\hat{x}$ component of spin pre-selected in the $+\frac{1}{2}$ state. The final state is post-selected in the $+\frac{1}{2}$ in a direction $\hat{\xi}$ oriented at an angle α with respect to $\hat{x}$ and transverse to the direction of propagation (see Fig. 1). The operator $\widehat{C}$ is given by

$$\widehat{C} \equiv \hat{\sigma}_x + \hat{\sigma}_\xi = 2\cos(\alpha/2)\hat{\sigma}_\theta \tag{14}$$

where $\theta = \alpha/2$ is the angle that bisects $\hat{x}$ and $\hat{\xi}$. Since the expectation values of both $\hat{\sigma}_x$ and $\hat{\sigma}_\xi$ are known to equal 1 for systems which pass both the pre- and

post-selection this equation can be solved for the expectation value of $\hat{\sigma}_\theta$:

$$(\sigma_\theta)_w = [\cos(\alpha/2)]^{-1} . \tag{15}$$

The w subscript denotes that this value is the weak value of the operator. $(\sigma_\theta)_w$ is precisely equal to the weak value defined by Eq. 2. As σ approaches π, the weak values becomes extremely large. If the Stern-Gerlach device which performs the weak measurement is oriented to measure the spin component in the θ direction, then the momentum change in the beam will reflect this large value. When the limitations of Eqs. 11 and 12 are met, the resulting distribution of particles will be centered around the weak value $(\sigma_\theta)_w$. The physical basis of the limitation on the size of the weak value is clear. Once the weak value becomes sufficiently large, the coupling to the measuring device cannot be neglected. Therefore, the measurement is no longer weak.

4. Experiment

Recently an optical experiment was proposed[2] and performed[6] which demonstrated a measurement of the weak value of an operator. A laser beam replaced the beam of spin-$\frac{1}{2}$ particles and the pre- and post-selections were performed by optical polarizers. The weak measurement was performed by a birefringent crystalline quartz plate. The polarization dependent index of refraction of the birefringent plate caused a small spatial shift between the positions of the centroids of the two orthogonally polarized components of the laser beam. The difference in shift for the ordinary and extraordinary rays was much less than the beam waist of the laser, thus satisfying the condition of weakness.

The experimental configuration is shown in Fig. 2. The beam from a frequency stabilized He-Ne laser was collimated to a beam waist of 1.52 mm. A 400 mm focal length lens focused the beam onto the post-selection polarizer. The pre-selection was performed by a polarizer with its axis oriented at $\alpha = \pi/4$ with respect to the x-axis. The weak measurement was performed by passing the laser beam through a birefringent plate oriented with the optic (extraordinary) axis along the x-axis. The plane of the plate was rotated about the optic axis by an angle θ with respect to the propagation (z) axis. This plate produced a small relative shift in the y direction between the two orthogonal polarization components. The post-selection was performed with a second polarizer oriented at an angle β with respect to the x-axis. The location of the second polarizer determined the beam waist at the interference point, $w_0 = 55$ μm. Immediately after the polarizer the light was projected by a short focal length lens onto a photodiode which was scanned across the distribution.

In analogy to the spin-$\frac{1}{2}$ particles, the polarization of the photons replaces the spin state of the particles. Instead of up and down spin states, the horizontal and vertical polarization directions form the orthogonal states of the system. The weak value of the displacement in the direction bisecting the pre- and post-selection is

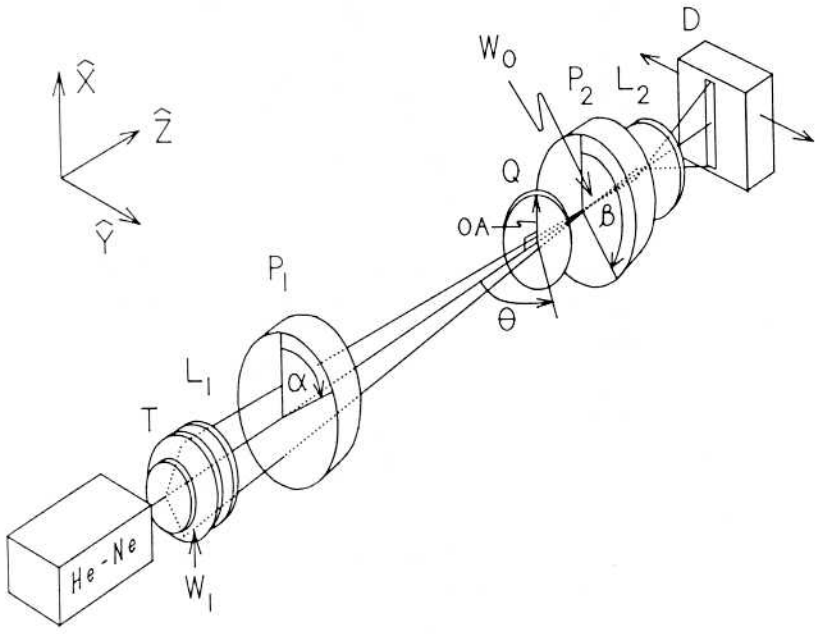

Fig. 2. Schematic diagram of the apparatus. The output of a frequency stabilized He-Ne laser is collimated, focused and polarized at an angle α relative to the x-axis by telescope T, lens L_1, and polarizer P_1, respectively. A birefringent crystalline quartz plate Q with optic axis (OA) aligned along the x-axis is located near the focus of the laser beam. Q performs a weak measurement by spatially separating the ordinary and extraordinary polarization components along the y-axis by a distance small compared to the focused beam waist w_0. Polarizer P_2, whose axis makes an angle β with the x-axis, post-selects the final polarization state. Lens L_2 expands the image onto a photo-detector D. D is scanned along the y-axis, recording the intensity function $I(y)$.

given by

$$(D_{\mathrm{bi}})_{\mathrm{w}} \simeq \frac{a}{2} \frac{1}{[\cos(\beta - \alpha)]} \tag{16}$$

where a is the actual displacement between the two polarizations and the displacement eigenvalues are $\pm 1/2a$. The weak measurement was performed along the y-axis, which did not necessarily bisect the pre- and post-selection. The more general expression for the weak value along the y-axis as a function of α and β is

$$(D_y)_{\mathrm{w}} \simeq \frac{a}{2} \frac{\cos(\beta + \alpha)}{\cos(\beta - \alpha)}. \tag{17}$$

Since $\beta - \alpha$ is nearly $\pi/2$ for the interesting case and $\alpha = \pi/4$ for this experiment, we can define $\varepsilon = \beta - \alpha - \pi/2$ where ε measures the deviation from orthogonality. In terms of ε the total displacement is

$$(D_y)_{\mathrm{w}} \simeq \frac{a}{2} \cot(\varepsilon). \tag{18}$$

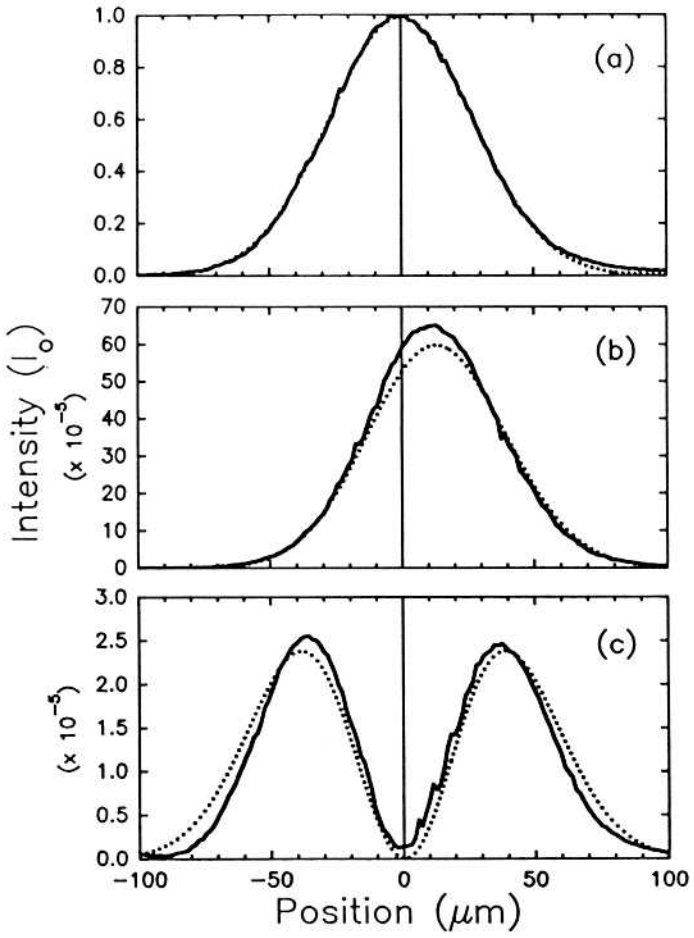

Fig. 3. Experimental data and fits to the data using Eq. 19. The horizontal axis is scaled to measure y at the position of the focus of the laser beam. The recorded intensity is due to a superposition of the two initial Gaussian distributions which are separated by a small distance $a \approx 0.64$ μm, which is much less than the Gaussian beam waist, $w_0 = 55$ μm. (a) $\alpha = \beta = \pi/4$, corresponding to aligned polarizers. In this case the measured intensity is the result of constructive addition of two Gaussian distributions. The dotted line, which almost perfectly overlaps the data, is the fit. (b) $\alpha = \pi/4$, $\beta = 3\pi/4 + 2.2 \times 10^{-2}$, corresponding to a measurement of the weak value. The centroid of the distribution is shifted by $A_w = 12$ μm, which is approximately $20a$. (c) $\alpha = \pi/4$, $\beta = 3\pi/4$, corresponding to crossed polarizers, or orthogonal initial and final states. In this case, A_w no longer corresponds to the shift. The separation of the two peaks is $\sim 120a$.

Figure 3 shows the data for three relative positions of the polarizers. Figure 3a is the case when both polarizers axes are parallel, $\alpha = \beta = \pi/4$, for which Eq. 18 gives $A_w = 0$. This zero value is due to the equal population of both polarization states. Figure 3b shows data for $\varepsilon = 0.022$. The centroid of the distribution is shifted by approximately $20a$. The criteria for identifying the shifted centroid with

the weak value are fulfilled so that the magnitude of this shift equals the weak value A_w. Figure 3c shows data for $\varepsilon = 0$. In this case, the weak value no longer represents anything physical. As $\varepsilon \to 0$, $A_w \to \infty$ violating the requirement that $A_w \ll w_0$, which is the optical equivalent of Eq. 11. All three sets of data were fit using the exact distribution calculated from classical interference:

$$I(y) = I_0 \left[\cos(\alpha)\cos(\beta)\exp\left(\frac{-(y+a/2)^2}{w_0^2}\right) + \sin(\alpha)\sin(\beta)\exp\left(\frac{-(y-a/2)^2}{w_0^2}\right)\right]^2 . \tag{19}$$

Though this expression is purely classical, it exhibits the same interference induced shift as the quantum system.

From knowledge of the indices of crystalline quartz[12] and geometric factors we calculate $a = 0.64$ μm which is approximately equal to the wavelength of the light used. From the fits to the data we were able to extract values of 0.65 ± 0.05 μm and 0.62 ± 0.04 μm for the data in Fig. 3b and 3c, respectively. Although in theory we should have also been able to extract a from the data in Fig. 3a, the lack of detector resolution, among other factors, precluded it.

5. Application to Practical Measurements

The amplification produced by the post-selection process may be useful for practical measurements of weak effects. For example, in the optical experiment previously described, the birefringence of quartz was accurately measured. However, the destructive interference of the unresolved eigenstates produced by the post-selection process causes a loss in signal intensity, in addition to the strong modulation in signal shape. Therefore, it is not obvious *a priori* that a small parameter (a in the experiment above) can be more accurately extracted from a signal resulting from the destructively interfered distribution than from the constructively interfered distribution which is obtained when the pre- and post-selected states are the same.

In order to answer this question, we compared measurements where two eigenvalues are unresolved using three separate techniques: a constructively interfered measurement (CI) where $\langle \Psi_{in} | \Psi_f \rangle = 1$, a measurement of the weak value (WV) where $\langle \Psi_{in} | \Psi_f \rangle \ll 1$, but where the restrictions imposed by Eqs. 11 and 12 are still satisfied, and a destructively interfered measurement (DI) where $\langle \Psi_{in} | \Psi_f \rangle = 0$. In terms of the quantities defined in Sec. 4, CI corresponds to $\alpha = \beta = \pi/4$, DI corresponds to $\alpha = \pi/4$, $\beta = 3\pi/4$, and WV corresponds to $\alpha = \pi/4$ and $\beta = 3\pi/4 + \varepsilon$, with ε such that $A_w = 1/2a \cot(\varepsilon)$. In the case of the CI measurement, the recorded signal will have a large amplitude, but the effect of the small interaction with the weak measuring device will produce little change in the recorded signal shape. In the DI case, the recorded signal will have small amplitude, but the signal shape will be strongly affected.

For each of the three cases, the expected signal was numerically generated for various values of the experimental parameters. Random noise was then added to these signal distributions. Only statistical noise representing random fluctuations in the detected signal intensity was included; noise due to systematic effects was not accounted for. Therefore, the numerically generated data correspond to ideal "shot-noise" limited "experiments". This "noisy" data was then fit to the exact expression for the final distribution, Eq. 19, and a value for the eigenvalue separation a was extracted. Since the relative noise is proportional to $I^{-1/2}$, where I is the measured signal intensity, the CI data has the smallest relative noise, and the DI data has the greatest.

The initial pre-selected distribution was a Gaussian with width parameter $w_0 = 1$ and height $I_0(N, \Delta y)$, where N is the total number of particles in the initial distribution, Δy is the bin width of data points on the y-axis, and I_0 is defined by the sum over the data bins as $N = \Sigma_i I_0 \exp(-y_i^2/w_0^2)$. Equation 19 and the values of I_0, a, α, and β determined the exact post-selected distribution. Statistical noise was added to each data set using a pseudo-random routine to generate a Poissonian deviate.[13] The resulting distribution was fit to Eq. 19 using the Marquart-Levenberg method.[13] The fitted parameters were a and the initial center of the distribution y_0, while all other parameters were fixed. The resulting value for a was compared for the CI, DI and WV cases. This procedure was repeated sixteen times for each combination of N, Δy, and a and the mean value $\bar{a}$ and the deviation from the mean δa, were calculated.

Figure 4 shows plots of numerically generated CI, DI and WV data and the corresponding best fit curves for the case where $N = 10^7$, $a = 0.01$, and $\Delta y = 0.1$. Because of the large value of N, the CI data shown in Fig. 4a has small relative noise and the fit to the data is almost indistinguished from the data itself. Figure 4b shows a measurement of the weak value, where $A_w = 31.6a$. In this case, the signal size is significantly smaller because of the nearly complete cancellation by the destructive interference. The noise is now readily visible. Figure 4c shows data corresponding to the DI case. Again, the noise is a significant fraction of the signal size. For the three cases, the fitted values for a were $a_{CI} = 0.0043$, $a_{WV} = 0.0096$, and $a_{DI} = 0.0098$, which should be compared to the exact value $a = 0.01$. Therefore, the DI case gave the most accurate and the CI data gave the least accurate measure of a.

This procedure was repeated for 168 different combinations of the parameters N, a, Δy and A_w. N was allowed to range between 10^6 and 10^{12}, a between 0.001 and 0.1, A_w between $100a$ and $10a$, and Δy between 1 and 0.01. Certain combinations of these parameters were eliminated because the interfered signal size was too small ($I(y)_{max} < 1$ for $\alpha = \pi/4$, $\beta = 3\pi/4$) and others were eliminated because they did not fulfill the weakness criteria (Eqs. 11 and 12). In each of the 168 cases $\delta a_{DI} < \delta a_{WV} < \delta a_{CI}$ and $|a_{DI} - a| < |a_{WV} - a| < |a_{CI} - a|$. A sample of the results are displayed in Table 1. In all cases, the accuracy of the measurement

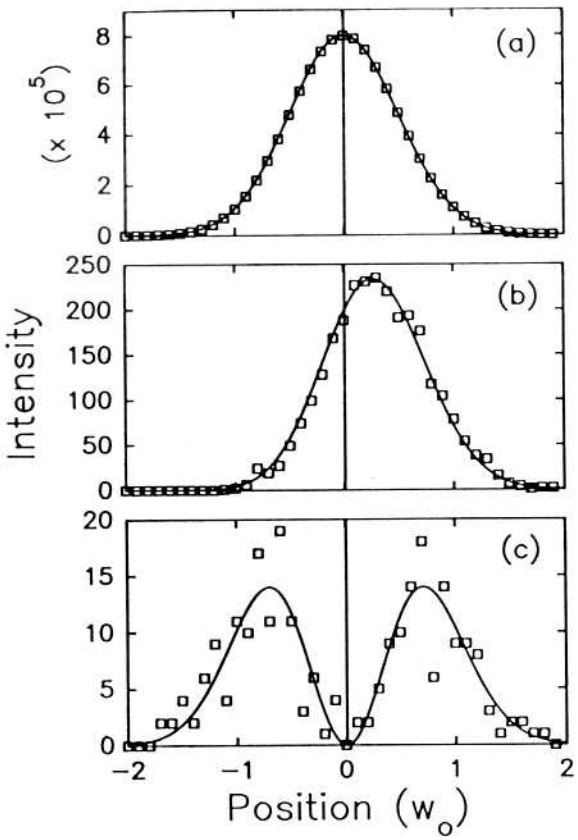

Fig. 4. Numerically generated data and fits. The boxes represent the data which were generated by computer by adding pseudo-random noise to the exact post-selected distribution calculated from Eq. 19. The lines are best fits of Eq. 19 to the data, with the eigenvalue separation a as the fitted parameter. The parameters are $I_0 = 8 \times 10^5$, $\Delta y = 0.1$, $w_0 = 1.0$, and $a = 0.01$. (a) $\alpha = \beta = \pi/4$, corresponding to a constructive interference (CI) measurement. The statistical noise is a small fraction of the signal. The best fit value for the eigenvalue spacing is $a = 0.0043$. (b) $\alpha = \pi/4$, $\beta = 3\pi/4 + 0.0632$, corresponding to a measurement of the weak value (WV) with $A_w = 31.6a$. The best fit gives $a = 0.0096$ (c) $\alpha = \pi/4$, $\beta = 3\pi/4$, corresponding to a destructive interference (DI) measurement. Even though the statistical noise is a significant fraction of the signal, the DI measurement produced the most accurate measurement $a = 0.0098$.

improved as the size of the weak value was increased, or equivalently, as the post-selected state became more orthogonal to the pre-selected one.

6. Conclusion

The weak value of an operator has been shown to be a physically measurable quantity and a measurement of the weak value has been realized in an optical experiment. Weak values can be understood through standard quantum mechanical analysis as the result of interference of the eigenstates of an operator. When the weakness

Table 1. Typical results of the numerical simulation. The column labelled $\bar{a}$ for the CI, DI, and WV cases is the average fitted value of a for 16 numerically generated "noisy" data sets for each given combination of parameters. The following parameters were varied: N, the total number of particles in the experiment; Δy, the step size between data points along the y-axis; a, the eigenvalue spacing; and A_w, the size of the weak value, which in turn determines ε through $A_w = 1/2a \cot(\varepsilon)$. $\delta a/\bar{a}$ is the fractional RMS deviation from the mean for the 16 trials. As A_w increases and ε decreases ($\varepsilon = 0$ for DI), the accuracy of the measurement increases.

N	Δy	A_w/a	$\bar{a}$	$\lvert\delta a\rvert/\bar{a}$	
1×10^6	0.1		0.0100	—	exact
			0.022	2.5×10^0	CI
		10	0.011	5.5×10^{-1}	WV
			0.0098	9.2×10^{-2}	DI
1×10^7	0.1		0.01	—	exact
			0.0078	1.2×10^0	CI
		10	0.01	1.3×10^{-1}	WV
			0.01	3.3×10^{-2}	DI
1×10^8	0.1		0.0032	—	exact
			0.0081	2.7×10^0	CI
		31.6	0.0028	4.9×10^{-1}	WV
			0.0032	3.1×10^{-2}	DI
1×10^8	0.032		0.0032	—	exact
			0.0082	3.0×10^0	CI
		31.6	0.0030	1.6×10^{-1}	WV
			0.0031	3.4×10^{-2}	DI
1×10^{10}	0.1		0.001	—	exact
			0.0024	2.5×10^0	CI
		10	0.00094	4.4×10^{-1}	WV
			0.0010	9.6×10^{-3}	DI
1×10^{10}	0.1		0.001	—	exact
			0.0019	2.2×10^0	CI
		100	0.00099	6.4×10^{-2}	WV
			0.0010	7.6×10^{-3}	DI
1×10^{12}	0.01		0.001	—	exact
			0.0011	8.1×10^{-1}	CI
		10	0.0010	4.7×10^{-2}	WV
			0.0010	8.4×10^{-4}	DI
1×10^{12}	0.01		0.01	—	exact
			0.01	1.1×10^{-2}	CI
		10	0.01	5.6×10^{-4}	WV
			0.01	1.2×10^{-4}	DI

condition is satisfied by the measurement, the sum of small shifts can be replaced by a single shift equal to the weak value. Under some conditions this average shift can

be much larger than any of the small shifts which produce it. Using a model which includes random noise, we have shown that this effect may be a useful technique for amplifying and detecting small effects. Even when the weak value becomes unphysical in the limit of orthogonal initial and final states, the interference due to the weak measurement still produces shifts which can be large compared to the eigenvalue separation. In this limit the intensity is a strong function of a which can be used to make accurate measurements of small effects. The unique properties of weak values is a continuing field of study.[14]

Acknowledgement

The authors thank Professors P. M. Stevenson, I. M. Duck, and E. C. G. Sudarshan for suggesting the experiment to us. This work was partially supported by the Robert A. Welch Foundation, the NSF, and the Shell Foundation. R. G. Hulet is an Alfred P. Sloan Research Fellow.

References

1. Y. Aharonov, D. Z. Albert, and L. Vaidman, *Phys. Rev. Lett.* **60**, 1351 (1988).
2. I. M. Duck, P. M. Stevenson, and E. C. G. Sudarshan, *Phys. Rev.* **D40**, 2112 (1989).
3. Y. Aharonov and L. Vaidman, *Phys. Rev.* **A41**, 11 (1990).
4. J. M. Knight and L. Vaidman, *Phys. Lett.* **A143**, 357 (1990).
5. See the following Comments, A. J. Leggett, *Phys. Rev. Lett.* **62**, 2325 (1989); A. Peres, *ibid.* **62**, 2326 (1989); and the Reply by A. Aharonov and L. Vaidman, *ibid.* **62**, 2327 (1989).
6. N. W. M. Ritchie, J. G. Story, and R. G. Hulet, *Phys. Rev. Lett.* **66**, 1107 (1991).
7. J. von Neumann, *Mathematische Grundlagen der Quantenmechanik* (Springer, Berlin, 1932) [English translation: *Mathematical Foundations of Quantum Mechanics* (Princeton University Press, 1955)]. See also W. E. Lamb, *Phys. Today* **22** (4), 23 (1969).
8. A. Peres, *Phys. Rev.* **D39**, 2943 (1989).
9. Y. Aharonov, D. Albert, A. Casher, and L. Vaidman, *Phys. Lett.* **A124**, 199 (1987).
10. L. Vaidman, Y. Aharonov, and D. Albert, *Phys. Rev. Lett.* **58**, 1385 (1987).
11. Y. Aharanov, P. G. Bergman, and J. L. Lebowitz, *Phys. Rev.* **B134**, 1410 (1964).
12. F. F. Martens, *Ann. Physik* **6**, 603 (1901). The indices, n_e and n_0 at 633 nm, were calculated from the curves $n_0 = 1.60324 - 1.585 \times 10^{-4}\lambda + 9.907 \times 10^{-8}\lambda^2$ and $n_e = 1.61258 - 1.582 \times 10^{-4}\lambda + 9.768 \times 10^{-8}\lambda^2$ which came from fitting Martens values near 633 nm.
13. W. H. Press, B. P. Flannery, S. A. Teukolsky, and W. T. Vetterling, *Numerical Recipes: The Art of Scientific Computing* (Cambridge University Press, 1987).
14. Y. Aharonov, J. Anandan, S. Popescu, and L. Vaidman, *Phys. Rev. Lett.* **64**, 2965 (1990).